



QUANTITATIVE OPTICAL MANIPULATION OF A SINGLE 4-CYANO-4'-PENTYLBIPHENYL MICRODROPLET IN WATER FOR ACTUATING AND SENSING APPLICATIONS



MUHAMAD SAFUAN BIN MAT YENG @ MAT ZIN

SULTAN IDRIS EDUCATION UNIVERSITY

2024



QUANTITATIVE OPTICAL MANIPULATION OF A SINGLE
4-CYANO-4'-PENTYLBIPHENYL MICRODROPLET IN
WATER FOR ACTUATING AND SENSING
APPLICATIONS

MUHAMAD SAFUAN BIN MAT YENG @ MAT ZIN

THESIS PRESENTED TO QUALIFY FOR A
DOCTOR OF PHILOSOPHY

FACULTY OF SCIENCE AND MATHEMATICS
SULTAN IDRIS EDUCATION UNIVERSITY

2024



Please tick (✓)
Project Paper
Masters by Research
Master by Mixed Mode
PhD

/

INSTITUTE OF GRADUATE STUDIES
DECLARATION OF ORIGINAL WORK

This declaration is made on the6.....day of.....FEB.....20.24...

i. Student's Declaration:

I, MUHAMAD SAFUAN BIN MAT YENG @ MAT ZIN, P20201000025, FSM (PLEASE INDICATE STUDENT'S NAME, MATRIC NO. AND FACULTY) hereby declare that the work entitled QUANTITATIVE OPTICAL MANIPULATION OF A SINGLE 4-CYANO-4'-PENTYLBIIPHENYL MICRODROPLET IN WATER FOR ACTUATING AND SENSING APPLICATIONS is my original work. I have not copied from any other students' work or from any other sources except where due reference or acknowledgement is made explicitly in the text, nor has any part been written for me by another person.

Signature of the student

ii. Supervisor's Declaration:

I ASSOC. PROF. DR. Ts. SHAHRUL KADRI BIN AYOP (SUPERVISOR'S NAME) hereby certifies that the work entitled QUANTITATIVE OPTICAL MANIPULATION OF A SINGLE 4-CYANO-4'-PENTYLBIIPHENYL MICRODROPLET IN WATER FOR ACTUATING AND SENSING APPLICATIONS (TITLE) was prepared by the above named student, and was submitted to the Institute of Graduate Studies as a partial/full fulfillment for the conferment of DOCTOR OF PHILOSOPHY (PHYSICS) (PLEASE INDICATE THE DEGREE), and the aforementioned work, to the best of my knowledge, is the said student's work.

6/2/2024

Date

Signature of the Supervisor

Prof. Madya Ts. Dr. SHAHRUL KADRI BIN AYOP



**INSTITUT PENGAJIAN SISWAZAH /
INSTITUTE OF GRADUATE STUDIES**

**BORANG PENGESAHAN PENYERAHAN TESIS/~~DISERTASI/LAPORAN KERTAS PROJEK~~
DECLARATION OF THESIS/~~DISSERTATION/PROJECT PAPER FORM~~**

Tajuk / Title: QUANTITATIVE OPTICAL MANIPULATION OF A SINGLE 4-CYANO-4'-PENTYLBIPHENYL MICRODROPLET IN WATER FOR ACTUATING AND SENSING APPLICATIONS

No. Matrik / Matric's No.: P20201000025

Saya / I / : MUHAMAD SAFUAN BIN MAT YENG @ MAT ZIN
(Nama pelajar / Student's Name)

mengaku membenarkan Tesis/~~Disertasi/Laporan Kertas Projek~~ (Kedoktoran/~~Sarjana~~)* ini disimpan di Universiti Pendidikan Sultan Idris (Perpustakaan Tuanku Bainun) dengan syarat-syarat kegunaan seperti berikut:-
acknowledged that Universiti Pendidikan Sultan Idris (Tuanku Bainun Library) reserves the right as follows:-

1. Tesis/~~Disertasi/Laporan Kertas Projek~~ ini adalah hak milik UPSI.
The thesis is the property of Universiti Pendidikan Sultan Idris
2. Perpustakaan Tuanku Bainun dibenarkan membuat salinan untuk tujuan rujukan dan penyelidikan.
Tuanku Bainun Library has the right to make copies for the purpose of reference and research.
3. Perpustakaan dibenarkan membuat salinan Tesis/Disertasi ini sebagai bahan pertukaran antara Institusi Pengajian Tinggi.
The Library has the right to make copies of the thesis for academic exchange.
4. Sila tandakan (✓) bagi pilihan kategori di bawah / Please tick (✓) for category below:-

☐ **SULIT/CONFIDENTIAL**

Mengandungi maklumat yang berdarjah keselamatan atau kepentingan Malaysia seperti yang termaktub dalam Akta Rahsia Rasmi 1972. / Contains confidential information under the Official Secret Act 1972

☐ **TERHAD/RESTRICTED**

Mengandungi maklumat terhad yang telah ditentukan oleh organisasi/badan di mana penyelidikan ini dijalankan. / Contains restricted information as specified by the organization where research was done.

☒ **TIDAK TERHAD / OPEN ACCESS**


(Tandatangan Pelajar/ Signature)


(Tandatangan Penyelia / Signature of Supervisor)
& (Nama & Cop Rasmi / Name & Official Stamp)

Tarikh: 8 FEBRUARY 2024


Prof. Madya Ts. Dr. SHAHRUL KADRI BIN AYOP
Universiti Pendidikan Sultan Idris
bit.ly/kadrimy

Catatan: Jika Tesis/Disertasi ini SULIT @ TERHAD, sila lampirkan surat daripada pihak berkuasa/organisasi berkenaan dengan menyatakan sekali sebab dan tempoh laporan ini perlu dikelaskan sebagai SULIT dan TERHAD.

Notes: If the thesis is CONFIDENTIAL or RESTRICTED, please attach with the letter from the organization with period and reasons for confidentiality or restriction.

ACKNOWLEDGEMENT

Alhamdulillah, first and foremost, I would like to thank Allah SWT for everything. Without his blessing, I might not have been able to complete this work. My most excellent commitment and appreciation is to my supervisors, Assoc. Prof. Dr. Ts. Shahrul Kadri bin Ayop and Dr. Izan Roshawaty binti Mustapa, thank you for your guidance and brilliant insights in my journey toward completing this thesis. Your excellent care and motivating support have helped me on this challenging but healing journey. Many thanks to the Faculty of Science and Mathematics staff, who are directly or indirectly involved in this research. Without their help, this thesis would not have been possible in its current form. I also thank the Ministry of Higher Education Malaysia (MOHE) especially MyBrainSc Scholarship for funding my PhD studies. I would also like to thank the Photo-Physics System Laboratory, Research Institute for Electronic Science (RIES) at Hokkaido University, especially Prof. Dr. Keiji Sasaki, Dr. An-Chieh Cheng and Dr. Christophe Pin for supervising and guiding my research work for 3 months research attachment. Thank you to all my friends, Siti Azizah, Nur Izzati, Nur Farah Nadia, Wong Yeong Yi, Anis Nabila and Faiz Farhan, for all the beautiful and fun memories. Finally, I want to thank my family, who have always been supportive and kind.



ABSTRACT

The study aims to formulate the production of 4-cyano-4'-pentylbiphenyl (5CB) microdroplets within a suitable range to be optically trapped, to optically trap a single 5CB microdroplet in water within a suitable size range, to optically micro-control the microdroplet using a circularly polarized laser, and to quantitatively determine factors affecting the optical manipulation of the microdroplet. 0.5 μL 5CB was mixed with the deionized water and sonicated to produce bipolar and radial 5CB microdroplet suspensions. The 5CB microdroplet was observed under optical microscopy and its size distribution was measured using ImageJ, while its stability was measured using UV-Vis spectroscopy. A linearly polarized laser beam of 976 nm wavelength was used to optically trap a single 5CB microdroplet in water at a specific laser power density. A circularly polarized laser beam was used to optically trap a single 5CB microdroplet to study its orientation control, rotatability control, and simultaneous translation micro-control. A single 5CB microdroplet was trapped and introduced to the cetyltrimethylammonium bromide (CTAB) solution to study its visual internal configuration change and optical signal. The finding shows that the size distribution of 5CB microdroplet suspension decreased with time. However, it was stable and sustained in 1-hour monitoring. The 5CB microdroplet could be linearly translated and rotated, enabling the simultaneous translation-micro-control. The corner frequency (f_c) and angular speed (ω) showed an increasing trend with optical power density (P) increment. Exposing CTAB solution to the trapped 5CB microdroplet changed its internal configuration from bipolar to radial, optical signal and displacement variance (σ^2). In conclusion, the trapped 5CB microdroplet could be micro-controlled as a microactuator while f_c , ω , and σ^2 measurements were characteristics of microdroplet-based sensors. This study implies that the optical trapping of a single 5CB microdroplet in water has potential for prospective actuating and sensing applications.





PEMANIPULASIAN OPTIK KUANTITATIF BAGI SATU MIKROTITISAN 4-SAIANO-4'-PENTILBIFENIL TUNGGAL DALAM AIR UNTUK APLIKASI PENGGERAKAN DAN PENDERIAAN

ABSTRAK

Kajian ini bertujuan untuk merumuskan penghasilan mikrotitisan 4-saiano-4'-pentilbifenil (5CB) dalam julat yang sesuai untuk diperangkap secara optik, untuk memerangkap secara optik satu mikrotitisan 5CB tunggal di dalam air dalam julat saiz yang sesuai, untuk memikrokawal mikrotitisan tersebut menggunakan alur laser berkutub bulat, dan untuk menentukan secara kuantitatif faktor-faktor yang mempengaruhi pemanipulasian optik mikrotitisan tersebut. 0.5 μL 5CB telah dicampur dengan air ternyahion dan disonikasi dalam tempoh masa yang khusus untuk menghasilkan ampaian mikrotitisan 5CB dwikutub dan jejarian di dalam air. Mikrotitisan 5CB telah diperhatikan melalui mikroskopi optik dan taburan saiznya diukur menggunakan ImageJ manakala kestabilannya diukur menggunakan spektroskopi UV-Vis. Satu alur laser berkutub linear yang mempunyai panjang gelombang 976 nm digunakan untuk merangkap secara optik satu mikrotitisan 5CB tunggal pada ketumpatan kuasa laser tertentu. Alur laser berkutub bulat pula telah digunakan untuk merangkap secara optik satu mikrotitisan 5CB tunggal bagi mengkaji kawalan orientasi, kawalan kebolehputaran, dan translasi mikrokawalan serentak mikrotitisan tersebut. Satu mikrotitisan 5CB tunggal juga diperangkap dan didedahkan kepada larutan setiltrimetilammonium bromida (CTAB) untuk mengkaji perubahan konfigurasi dalaman secara visual dan signal optik mikrotitisan tersebut. Dapatan menunjukkan bahawa taburan saiz ampaian mikrotitisan 5CB berkurang dengan masa. Akan tetapi, mikrotitisan tersebut stabil dan kekal dalam pemantauan selama 1 jam. Mikrotitisan 5CB tersebut juga boleh diperangkap secara linear dan diputar, membolehkan translasi-mikrokawalan serentak. Frekuensi penjuru (f_c) dan kelajuan sudut (ω) menunjukkan trend yang meningkat dengan peningkatan ketumpatan kuasa laser P . Pendedahan larutan CTAB terhadap mikrotitisan 5CB yang diperangkap telah menukarkan konfigurasi dalaman daripada dwikutub kepada jejarian, isyarat optik dan sesaran varians (σ^2) mikrotitisan tersebut. Kesimpulannya, mikrotitisan 5CB tunggal yang diperangkap boleh dimikrokawal sebagai mikropenggerak manakal pengukuran f_c , ω , dan σ^2 pula merupakan ciri-ciri penderia berasaskan mikrotitisan. Kajian ini menunjukkan bahawa perangkap optik satu mikrotitisan 5CB tunggal dalam air berpotensi untuk prospektif aplikasi penggerakan dan penderiaan.





TABLE OF CONTENT

	Page
DECLARATION OF ORIGINAL WORK	ii
DECLARATION OF THESIS	iii
ACKNOWLEDGEMENT	iv
ABSTRACT	v
ABSTRAK	vi
TABLE OF CONTENT	vii
LIST OF TABLES	xii
LIST OF FIGURES	xiii
LIST OF SYMBOLS	xxvii
LIST OF CONSTANTS	xxviii
LIST OF ABBREVIATIONS	xxix
APPENDIX LIST	xxx
CHAPTER 1 INTRODUCTION	1
1.1 Research Background	1
1.2 Problem Statement	6
1.3 Research Objective	9
1.4 Significance of Research	10
1.5 Limitation of Research	11
1.6 Thesis Outline	13
1.7 Summary	14



CHAPTER 2	LITERATURE REVIEW	15
2.1	Introduction	15
2.2	Principle of Optical Tweezers	16
2.3	Optical Trapping Regimes	17
2.3.1	Rayleigh Regime	18
2.3.2	Mie Regime	19
2.4	Optical Stiffness Calibration of Optical Trapping	22
2.5	Optical Stiffness Calibration	28
2.5.1	Equipartition Theorem (ET)	29
2.5.2	Boltzmann Statistics (BS) Theorem	30
2.5.3	Power Spectrum Density (PSD) Theorem	32
2.5.4	Comparison between Boltzmann Statistics (BS), Equipartition Theorem (ET), and Power Spectrum Density (PSD)	34
2.6	Optical Torque	36
2.7	Cross-Polarization in Optical Tweezers	38
2.8	Optical Trapping of Solid Dielectric Particle	40
2.9	Optical Trapping of Soft Liquid Microdroplet	43
2.10	Liquid Crystal Introduction	47
2.11	Classification of Liquid Crystal	49
2.12	Effective Refractive Index (n_{eff}) of the Nematic LC	53
2.13	Nematic Liquid Crystal Internal Configuration	55
2.13.1	Flat Surface	56
2.13.2	Spherical Geometry	57
2.14	4-Cyano-4'-Pentylbiphenyl (5CB)	60

2.15	Technique for Microdroplet Production	61
2.16	Nematic Liquid Crystal Microdroplet Production	63
2.17	Distribution Size by Mechanical Technique	66
2.18	Microdroplet Internal Configuration Modification	71
2.19	Nematic Liquid Crystal Microdroplet Study Stability	75
2.20	Nematic Liquid Crystal Microdroplet Optical Trap	77
2.21	Nematic Liquid Crystal Microactuator	95
2.22	Nematic Liquid Crystal Sensor	99
2.22.1	Microdroplet-Based Sensor	102
2.22.2	Whispering Gallery Mode (WGM) Sensing	107
2.23	Summary	115

CHAPTER 3 METHODOLOGY 125

3.1	Introduction	125
3.2	Research Flow Chart	126
3.3	Optical Tweezers System [Phase 1]	129
3.3.1	Trapping Module	131
3.3.2	Observation Module	138
3.3.3	Detection Module	143
3.3.4	Optical Tweezers Performance Test	148
3.4	Preparation of 5CB Microdroplet Solution [Phase 2]	150
3.4.1	Bipolar 5CB Microdroplet Solution Preparation	151
3.4.2	Radial 5CB Microdroplet Solution Preparation	155
3.4.3	5CB Microdroplet Observation by Optical Microscopy	159
3.4.4	ImageJ Optical Microscope Calibration	161

3.4.5	ImageJ Distribution Size (r) Measurement	165
3.4.6	5CB Microdroplet Stability Measurement	173
3.5	The 5CB Microdroplet Micro-Control [Phase 3]	174
3.5.1	Microdroplet Internal Configuration Control	175
3.5.2	5CB Microdroplet Rotational Control	178
3.5.3	Translation and Polarization Control	180
3.5.4	Trajectory Analysis of 5CB Microdroplet	183
3.6	Corner Frequency (f_c) and Angular Speed (ω) Measurement [Phase 4]	188
3.6.1	Corner Frequency (f_c) Flowchart Analysis	188
3.6.2	5CB Microdroplet Radius (r) Measurement	191
3.6.3	Corner Frequency (f_c) Analysis	195
3.6.4	Angular Speed (ω) Measurement	201
3.6.5	5CB Microdroplet Angular Speed (ω) Analysis	203
3.7	Microdroplet Trapping in CTAB Solution [Phase 5]	204
3.7.1	5CB Microdroplet Trapping in CTAB Solution	206
3.7.2	Displacement Variance (σ^2) Analysis	209
3.8	Summary	212
CHAPTER 4	RESULTS AND DISCUSSION	213
4.1	Introduction	213
4.2	The Production of 5CB Microdroplet Suspension	214
4.2.1	Effect of Sonication Time on the Size of 5CB Microdroplet	214
4.2.2	5CB Microdroplet Suspension Stability in Water	223
4.3	Linearly Polarized Laser 5CB Microdroplet Trapping	229

4.4	5CB Microdroplet Orientation Control	233
4.5	Rotatability of 5CB Microdroplet	240
4.6	5CB Microdroplet Translational and Micro-control	242
4.7	Corner Frequency (f_c) Analysis	249
4.8	Angular Speed (ω) Analysis	262
4.9	Trapped 5CB Microdroplet Sensing Mechanism	279
4.9.1	5CB Microdroplet CTAB Sensing	281
4.10	Summary	287
CHAPTER 5	CONCLUSIONS AND RECOMMENDATION	290
5.1	Introduction	290
5.2	Conclusion	291
5.3	The Research Novelties	293
5.4	Implications	295
5.5	Recommendations	297
5.6	Summary	299
REFERENCES		301
APPENDICES		314



LIST OF TABLES

Table No.		Page
2.1	Comparison between Boltzmann Statistics (BS), Equipartition Theorem (ET), and Power Spectrum Density (PSD) calibration.	35
2.2	Advantages and disadvantages of previous research.	116
3.1	Module and Component of OTKB.	131
3.2	List of used laser current, power, and power density.	137
3.3	Measurement of length in unit pixels by ImageJ.	142
3.4	Measurement of length in unit pixels by ImageJ.	164
4.1	The comparison of 5CB microdroplet size produced from sonication.	221
4.2	Comparison of $\frac{f_c}{r}$ at P = 6.1 to 6.3 MW/cm ² for chloroform, toluene, 1,2-dichlorobenzene and 5CB microdroplets.	259
4.3	Comparison of density, refractive index, and solubility of Chloroform, Toluene, 1,2-dichlorobenzene, and 5CB.	261
4.4	Comparison of $\frac{\omega}{r}$ for bipolar 5CB reported by Murazawa and this study.	275
4.5	Comparison of $\frac{\omega}{r}$ for radial 5CB reported by Murazawa and this study.	276
4.6	Displacement variance (σ^2) at a particular time.	286





LIST OF FIGURES

Figure No.		Page
1.1	(Left) Laser trapping principle. (Right) Schematic representations for the trapping and assembly of nanoparticles, polymers, and molecular clusters. [Adapted from (Sugiyama et al., 2012).	3
1.2	5CB chemical structure. Adapted from (Yeng, Ayop, & Sasaki, 2022).	4
1.3	Liquid crystal internal configuration in a nematic liquid crystal microdroplet (a) bipolar and (b) radial. Observation under cross-polarization view [Adapted from ((Brasselet & Juodkazis, 2009)].	5
2.1	Forces exerting on a colloid microparticle near a focused beam. Adapted from (Konyshev & Byvalov, 2021).	16
2.2	The origin of the gradient force acting on a spherical particle near a non-focused (left) and focused (right) laser beam. Adapted from (Konyshev & Byvalov, 2021).	20
2.3	The F_r is acting on the trapped particle due to slight displacement from the laser trap center.	23
2.4	Linear graph of the trap stiffness versus beam powers (Aziz et al., 2016).	24
2.5	Trap stiffness as a function of laser power at the specimen plane, using the passive stiffness calibration method based on the power spectral density (Mohammad et al., 2014).	25
2.6	The optical stiffness graph against the chloroform microdroplet's size. Adapted from (Yusuf & Ayop, 2020).	27
2.7	Illustration of stuck bead sediment at the glass wall.	31
2.8	Microscopy images (top: brightfield, bottom: cross-polarized view correspond to the identical exact particles) of native corn starch granules (a and e), SMC60 particles (b and f), SMC65 particles (c and g), and SMC70 particles (d and h) in water (Wulff et al., 2020).	39



2.9	The developed system's optical trapping and manipulation of the 6 μm and 10 μm (Patel et al., 2021).	41
2.10	The graph of the x -axis position histogram for polystyrene microbead trapped in water for (a) p_1 and p_2 .	42
2.11	The optimal microdroplet number for optical trapping (Yusof et al., 2020).	44
2.12	f_c for various microdroplet sizes at a 6.3 MW/cm ² laser power density. The eye guides are drawn to indicate the trend of the f_c (Yusof et al., 2020).	45
2.13	The image of aerosol droplet optically trapped (a) 6.7 μm and (b) 2.0 μm (Taylor et al., 2005).	46
2.14	The molecular features of calamatic and discotic liquid crystals (Shen & Dierking, 2019).	49
2.15	Illustrates the thermotropic liquid crystal molecules arrangement the in the nematic, cholesteric, and smatic phases (Khoo, 2009).	50
2.16	The transition of the liquid crystal phase started from crystal to isotropic due to the heating process (Dierking & Al-zangana, 2017).	51
2.17	Schematic representation of the phase diagram of an amphiphilic surfactant in an isotropic solvent that forms lyotropic phases. (Dierking & Al-zangana, 2017).	52
2.18	Index ellipsoid for the case of uniaxial materials. (a) A plane perpendicular to the wave vector defines the plane of the electric field components experienced (n_o) and (n_{eff}). (b) The effective refractive index n_{eff} can be calculated with a geometric construction in the plane of incidence. Adapted from (Scharf, 2007).	53
2.19	The schematic diagram of the zenithal (θ) and azimuthal (φ) definition director angles to characterize the preferred orientation of a liquid crystal, set by alignment (easy axis) on a flat surface. Adapted from (Esteves et al., 2020).	56
2.20	(a) Planar alignment and (b) homeotropic director configuration of the liquid crystal molecules on the flat surface. \vec{N} is a vector orthogonal to the plane surface and \vec{n} is the director of the liquid crystal molecules. Adapted from (Esteves et al., 2020).	57
2.21	a) The illustration of bipolar configuration because of planar anchoring, (b) radial configuration because of homeotropic anchoring in droplet form. Adapted from (Esteves et al., 2020).	58



- 2.22 The snapshot of the polarized light microscopy images of nematic droplets (a) radial and (c) bipolar. The snapshot of bright field microscopy of (b) radial and (d) bipolar. The scale bar corresponds to 10 μm . Adapted from (Esteves et al., 2020). 59
- 2.23 5CB molecular structure (Khoo, 2009). 60
- 2.24 Method of making liquid crystal droplets. A: Vortex LC in water. B: Emulsifying liquid crystals using a homogenizer. C: Ultrasonic treatment of liquid crystals in water. D: Emulsifying liquid crystal in glycerol. E: Encapsulation of liquid crystals in polymeric microcapsules. F: Production of liquid crystal droplets using microfluidics. Adapted from (Wang et al., 2017). 62
- 2.25 An individual NLC microdroplet with a diameter of about 40 μm overhung out of one end of the microtube (Yan et al., 2017). 65
- 2.26 Micrographs of the stearic acid-doped 5CB microdroplets with different diameters (Duan et al., 2019). 65
- 2.27 Polarization optical microscopy images of 5CB droplets with different stirring times (a) 6 s; (b) 60 s; (c) 120 s; (d) 180 s; (e) 240 s; (f) relationship of the average diameter of droplets formed with stirring time. Scale bar: 500 μm . Adapted from (Niu et al., 2016). 67
- 2.28 The resulting mean droplet diameter (MDD) and polydispersity index (span) from different ultrasonic times of nanoemulsions. Adapted from (Asadinezhad et al., 2019). 69
- 2.29 The average droplet size is a function of exposure time on ultrasounds. Adapted from (Adamow et al., 2017). 70
- 2.30 The particle size of the gelation emulsion was treated with different sonication times. Adapted from (Li et al., 2023). 71
- 2.31 Concentration-diameter phase diagram of the 5CB liquid crystal droplets as a function of droplet diameter and SDS concentration. (a) All configurations, (b) bipolar, (c) monopolar and (d) radial are collectively represented (Shechter, Atzin, Moza, et al., 2020). 74
- 2.32 (a) Probability of a 5CB droplet having the internal radial alignment versus the concentration of cationic surfactant, 5CB internal configuration (b) radial and (c) bipolar (Murazawa, S. Juodkakis, 2005). 75
- 2.33 Visual image of bare E7 emulsion immediately after preparation (a), after storage 15 minutes and (c) 30 minutes respectively. Adapted from (Aery et al., 2023). 76



- 2.34 Variation of the diameter of 5CB microdroplets with time dispersed in PDMS. (Inset) Polarized optical microscope image of microdroplet with defects. Adapted from (Sofi & Dhara, 2019). 77
- 2.35 The schematic representation of polarization control of the incident trapping beam, the liquid crystal droplet was aligned according to the plane of polarization of the incident beam as shown in (a) to (e) (scale bar: 10 μm). Adapted from (Juodkazis et al., 1999). 79
- 2.36 (a)-(e) shows the spinning of the rotation of the liquid crystal droplet by circularly polarized light. Scale bar: 10 μm . Adapted from (Juodkazis et al., 1999). 80
- 2.37 Spinning radial 5CB droplet at 310 mW dragged floating droplet into orbiting motion. Scale bar, 10 μm . Adapted from (Murazawa, Juodkazis, & Misawa, 2005). 81
- 2.38 (a) Graph of rotation frequency, ω , of bipolar CB5 droplets against laser-power for diameters 3.2 μm (1), 2.5 μm (2), and 1.9 μm (3). (b) Graph of the rotation frequency of radial-5CB droplets against power for diameters 7.8 μm (1), 6.7 μm (2), 5.4 μm (3), and 4.8 μm (4). The lines act as guides for the eye. Adapted from (Murazawa, Juodkazis, & Misawa, 2005). 82
- 2.39 Sequences of the time evolution of POM images of an individual bipolar nematic 5CB droplet optically trapped by a linearly polarized trapping beam at (a) 130 mW (or 54 MW/cm²) and (b) 850 mW (or 360 MW/cm²). Adapted from (Usman et al., 2013). 84
- 2.40 Sequences of the time evolution of POM images of an individual bipolar nematic 5CB droplet optically trapped by a circularly (left-handed) polarized laser beam (a) at laser power 460 mW or 190 MW/cm², (b) an orbit of a tiny droplet around the rotating optically trapped droplet (the time is in seconds after the droplet starts to rotate), and (c) at laser power 940 mW or 390 MW/cm². (Usman et al., 2013). 85
- 2.41 The trapping location of the radial nematic liquid crystal (green rods) droplet shifted away from the droplet center under a linearly polarized light-trapping laser (red beam) (Phanphak et al., 2014). 88
- 2.42 A radial nematic liquid crystal droplet of 11.5 μm in diameter under the linearly polarized light optical trap of the following power: (a) without laser, (b) 28 mW, (c) 130 mW, (d) 246 mW. Adapted from (Phanphak et al., 2014). 89



- 2.43 A radial nematic liquid crystal microdroplet of 16.8 μm in diameter under 28 mW elliptical polarize optical light trap of the following elliptical angle: (a) without laser, (b) $\chi = 18^\circ$, (c) $\chi = 30^\circ$ and (d) $\chi = 45^\circ$. Adapted from (Phanphak et al., 2014). 90
- 2.44 An NLC droplet was found rotating clockwise under a linearly polarized laser trap at laser power 298 mW. The laser polarization direction was set at an angle $\beta = 135^\circ$ to the horizontal. Adapted from (Kiang-Ia et al., 2021). 93
- 2.45 The same 19- μm NLC droplet in Figure 2.44 rotated in the reverse direction under the same linearly polarized laser trap at a higher laser power of 635 mW. Adapted from (Kiang-Ia et al., 2021). 93
- 2.46 The graph of threshold laser power against droplet size clockwise and counterclockwise rotation. Adapted from (Kiang-Ia et al., 2021). 94
- 2.47 Optical micrograph of a micro-gear ($r = 4 \mu\text{m}$, $h = 14 \mu\text{m}$) rotating first to the left and then to the right under the control of the phase plate. Adapted with permission (Ito et al., 2012). 96
- 2.48 Experimental diagram of metalens-based optical tweezers. Adapted under the terms of the Creative Commons Attribution license (T-thienprasert, Limtrakul, Zentgraf, & Chattham, 2019). 97
- 2.49 Trapped bipolar and radial nematic liquid crystal microdroplet at $P = 30 \text{ mW}$ by circularly polarized light. Adapted under the terms of the Creative Commons Attribution (T-thienprasert, Limtrakul, Zentgraf, & Chattham, 2019). 98
- 2.50 Schematic diagram of the sensor using liquid crystal (Popov et al., 2017). 101
- 2.51 Liquid crystal droplet-based sensor for CA detection at varied concentrations. (a): 0 M; (b): 5 μM ; (c): 25 μM ; and (d): 50 μM . Scale bar: 200 μm . Adapted from (Niu et al., 2016). 104
- 2.52 The images of AIGG-anchored LC microdroplets incubated in PBS) with varied IgG concentrations at fixed liquid crystal microdroplets density (9×10^3 microdroplets per mL) anchored with 5 mg mL^{-1} of AIGG under polarized optical microscopy at 30 minutes contact time and room temperature. IgG concentration: (a) 10 ng mL^{-1} , (b) 20 ng mL^{-1} , and (c) 50 ng mL^{-1} . Adapted from (Lee et al., 2015). 105





2.53	Experiment setup to monitor trapped 5CB light emission. Adapted from (Humar & Mušević, 2011).	108
2.54	5CB droplet structure (Figure 2.54 (a)), 5CB bright field microscopy images (Figure 2.54 (b)), and 5CB crossed polarization view images (Figure 2.54 (c)), the light emission concentration dependence of 5CB microdroplets in water (Figure 2.54 (d)-(e)). Adapted from (Humar & Mušević, 2011).	110
2.55	Illustration of the experimental setup for sensing. Adapted from (Duan et al., 2019).	112
2.56	(a) The series stearic acid-dope 5CB microdroplet of polarized optical microscope (POM) images exposed to 200 pM copper (II) chloride in PBS solution at a specific time, (b) corresponding lasing spectra of POM images. Black dots represent the position of the WGM selected to monitor the spectral shifting of the droplet lasing emission. Scale bar: 20 μ m. Adapted from (Duan et al., 2019).	113
3.1	The research flowchart.	128
3.2	The actual (OTKB/M) system.	129
3.3	OTKB/M schematic diagram for optical trapping.	132
3.4	The snapshot of piezostage with labeled components.	133
3.5	The actual image of the butterfly laser diode used as the trapping laser source.	134
3.6	The image of a compact laser diode driver for controlling laser diode power.	134
3.7	The image of the laser power meter used in current-to-power calibration.	135
3.8	The plot of laser power (P) versus laser current (I) for calibrating the trapping laser in front of the objective lens.	136
3.9	A 100 \times magnification, 1.25 NA, 0.23 mm WD oil immersion objective.	138
3.10	Test cell under observation.	139
3.11	The live image of the CCD camera is displayed on the PC.	140
3.12	The front panel of the uploaded image of the calibration slide micro ruler in the ImageJ software.	141





3.13	The snapshot of the ImageJ front panel shows the straight-line measurement to determine the distance between two consecutive scales in pixels.	141
3.14	A QPD (PDQ80A, Thorlabs) is used for position sensing in OTKB/M.	144
3.15	The laser alignment procedure displays the position of the laser spot on the QPD via the APT user program.	144
3.16	The QPD diagram with four quadrant labels labeled a, b, c, and d.	145
3.17	Voltage waveform display on the Yokogawa DL6054 digital oscilloscope.	147
3.18	The graph of corner frequency (f_c) against laser optical power density (P) for optically trapped polystyrene microbeads in water.	149
3.19	The graph of optical stiffness (k_T) against laser optical power density (P) for optically trapped polystyrene microbeads in water.	149
3.20	The schematic diagram of the 5CB internal configuration (a) bipolar and (b) radial.	150
3.21	The snapshot of purchased 4-cyano-4'-pentylbiphenyl (5CB) in a glass bottle.	152
3.22	The schematic diagram of bipolar 5CB microdroplet suspension solution production.	152
3.23	The snapshot of the sonication process of liquid 5CB and deionized water mixture to produce a 5CB microdroplet suspension solution.	153
3.24	The snapshot of the mixture of the liquid 5CB and deionized water (a) before and (b) after the sonication process. The cloudy solution was formed after sonication, indicating the formation of the 5CB microdroplet suspension.	154
3.25	The image of the cell chamber (a) the 5CB microdroplet suspension was dropped on the glass slide, (b) the cover glass was assembled to the glass slide with two strips of double-sided tape, and (c) the schematic diagram of the cell chamber.	155
3.26	The effect of the CTAB solution volume on the formation of the radial 5CB microdroplet suspension.	156





3.27	The schematic diagram summarizes the production of the radial 5CB microdroplet suspension solution.	158
3.28	The actual image of the Inverted Metallurgical Microscope GX51 for observing and viewing purposes.	159
3.29	The schematic diagram of the Inverted Metallurgical Microscope GX51.	160
3.30	The actual particles (5CB microdroplet images) are seen at the specific focal plane.	161
3.31	Front Panel of ImageJ software.	161
3.32	(a) The image of the calibration slide ruler was observed under an inverted optical microscope (20× objective lens), (b) the front panel of an uploaded image of the calibration slide ruler in ImageJ software.	162
3.33	The snapshot of the straight-line measurement function is labeled with a dashed circle.	162
3.34	The zoomed Figure 3.32 (b) to demonstrates the Measurement of the distance between two scales of calibration ruler by a straight-line measurement. The obtained length was 40.608 pixels.	163
3.35	The snapshot of the (a) uncalibrated 5CB microdroplet image under an optical microscope and (b) front panel of uploaded 5CB microdroplets images by ImageJ software.	165
3.36	(a) Front panel for analysis and set scale function, (b) set scale front panel for calibration.	166
3.37	(a) Front panel for 8-bit image conversion and (b) image of 5CB microdroplets after 8-bit conversion.	167
3.38	The snapshot of the ImageJ front panel (a) front panel to impose bandpass filter, (b) FFT bandpass filter setting, and (c) the resulting image of the FFT bandpass filter imposed on the 5CB microdroplet image.	168
3.39	The snapshot of the (a) front panel for the Threshold option and (b) front panel for the “Threshold” setting.	169
3.40	(a) ImageJ automatic threshold highlighting the visible 5CB microdroplet with the red color, (b) the image of 5CB microdroplet after threshold measurement made by ImageJ.	170
3.41	(a) ImageJ front panel view for Analyze Particle option, Figure 3.41 (b) The front panel of Analyze Particles popup.	171





- 3.42 (a) Outlines the measured 5CB microdroplet area, and (b) the tabulated number and area of each measured 5CB microdroplet. 172
- 3.43 Schematic diagram of the 5CB microdroplet suspension (1.8 mL) for stability inspection by UV-Vis spectroscopy. 174
- 3.44 The actual image of the half-wave plate and (b) the position of the half-wave plate inserted in the optical path of the optical tweezers setup. 176
- 3.45 The schematic diagram shows the half-wave plate was oriented to angle θ , to the incoming perpendicular direction linearly polarized laser beam produced a horizontal linearly polarized laser beam to angle 2θ . Adapted from Standa Photonics. 177
- 3.46 The actual image of the quarter wave-plate and (b) the position of the quarter-wave plate inserted in the optical path of the optical tweezers setup. 178
- 3.47 The schematic diagram shows the quarter wave-plate was oriented to angle $\theta = 45^\circ$, to the incoming perpendicular direction linearly polarized laser beam produced a left-handed circularly polarized laser beam. Adapted from Standa Photonics. 179
- 3.48 The snapshot of the APT's User Software interface to control the translation of the piezostage. 180
- 3.49 The schematic diagram of the translation of the trapped particle by the piezostage control. 181
- 3.50 The front panel of the APT's User translates the piezostage $5\ \mu\text{m}$ to the right. 182
- 3.51 The schematic diagram of the translation and micro-control of the trapped 5CB microdroplet under a circularly polarized laser beam. The trapped 5CB microdroplet was rotated when the laser beam trapped it. 183
- 3.52 The screenshot of the Tracker Software to import the recorded video of the trapped 5CB microdroplet. 184
- 3.53 The snapshot of the calibrated recorded video of the trapped 5CB microdroplet by the Tracker Software. 185
- 3.54 The snapshot of the Tracker Software interface demonstrated the tracking procedure on the respected interest particle. 186
- 3.55 The snapshot of the Tracker Software's main front panel and the Autotracker function's front panel. 186





3.56	The snapshot of the Tracker Software, on the right side, shows the result of the tracked particle presented in the form of graph position in the x -direction and y -direction against time.	187
3.57	The snapshot of the trajectory data from the translation of the trapped particle.	188
3.58	The flowchart for measuring 5CB microdroplet radius (r) and corner frequency (f_c) using the ImageJ program and OSCal program.	190
3.59	The snapshot of the ImageJ Software front panel showed the uploaded and calibrated image of the trapped 5CB microdroplet.	191
3.60	The snapshot of the converted trapped 5CB microdroplet RGB image in Figure 3.59 to 8-bit.	192
3.61	(a) The snapshot of the Threshold front panel and (b) the corresponding display of the threshold measured on the trapped 5CB microdroplet image.	193
3.62	The snapshot of the image of the trapped 5CB microdroplet measured according to the set threshold in Figure 3.76 and (b) The snapshot of the Analyze Particles front panel to measure the area of the trapped 5CB microdroplet.	194
3.63	(a) The snapshot of the front panel shows the measured area of the trapped 5CB microdroplet image by ImageJ software. Figure 3.63 (b) The snapshot front panel shows the result of the area measured of the trapped 5CB microdroplet image by ImageJ Software.	194
3.64	Process of deleting headers inside Columns A1 to C15 of the signal data in Excel.	196
3.65	The interface of OSCal without any voltage signal data.	197
3.66	Selecting the directory of the data stored in the USB drive.	197
3.67	Data selection to upload into OSCal software.	198
3.68	The QPD voltage signal is displayed in the OSCal interface.	199
3.69	OSCal interface for Y-Power Spectrum of $3.0\ \mu\text{m}$ 5CB microdroplet.	200
3.70	The result of the power spectrum fitted with Lorentzian fitting.	201
3.71	The flowchart for the rotatability of trapped 5CB microdroplet analysis.	202



3.72	The graph is plotted from the QPD signal to determine the average time for a complete 2π rotation.	203
3.73	The flow chart of the optical trapping of a single 5CB microdroplet in CTAB solution.	205
3.74	The schematic diagram of the cell chamber (a) top view and (b) side view. The actual image of the cell chamber is shown in (c).	206
3.75	Schematic diagram of adding CTAB solution to the sample chamber edge.	208
3.76	The graph of voltage against time represents the trajectory of the trapped single 5CB microdroplet in water.	211
4.1	The snapshots of bipolar 5CB microdroplet suspension under optical microscopy sonicated at (a) $t = 1$ minute, (b) $t = 2$ minutes, (c) $t = 3$ minutes, and (d) $t = 10$ minutes for $V_{H2O} = 1$ mL. The inset shows the internal configuration of the bipolar 5CB microdroplet.	216
4.2	The snapshots of bipolar 5CB microdroplet suspension under optical microscopy sonicated at (a) $t = 1$ minute, (b) $t = 2$ minutes, (c) $t = 3$ minutes, and (d) $t = 10$ minutes for $V_{H2O} = 1$ mL. The inset shows the internal configuration of the radial 5CB microdroplet.	217
4.3	The average radius r , of 5CB microdroplets versus sonication time for (a) bipolar and (b) radial.	218
4.4	The absorption spectrum of 5CB for a 1-hour monitoring period.	225
4.5	The graph of peak versus time is in Figure 4.4 for (a) bipolar and (b) radial 5CB microdroplet suspension in water.	227
4.6	The graph of peak versus time in Figure 4.5 absorbance against time (a) bipolar 5CB and water, (b) radial 5CB, water, and CTAB.	228
4.7	Image sequence of the $0.7 \mu\text{m}$ bipolar 5CB microdroplet capturing into optical tweezers trap (red dash circle) at 0.2 MW/cm^2 . The red arrows indicate the polarization direction of the trapping laser.	230
4.8	Image sequence of the $1.0 \mu\text{m}$ radial 5CB microdroplet capturing into optical tweezers trap (red dash circle) at 0.2 MW/cm^2 . The red arrows indicate the polarization direction of the trapping laser.	231



- 4.9 The snapshot of 2.0 μm bipolar 5CB microdroplet trap at 0.2 MW/cm² at varied polarization direction, θ . The red arrows indicate the polarization direction of the trapping laser. 234
- 4.10 The snapshot of 2.0 μm bipolar 5CB microdroplet trap at 0.2 MW/cm² at varied polarization direction, θ under cross-polarized view. The red arrows indicate the polarization direction of the trapping laser. 234
- 4.11 The schematic diagram of 5CB molecules orientation inside the microdroplet to the polarization direction of linearly polarized light. The red arrows indicate the polarization direction of the trapping laser. 235
- 4.12 The snapshot of 3.3 μm radial 5CB microdroplet trap at 0.2 MW/cm² at varied polarization direction, θ . The red arrows indicate the polarization direction of the trapping laser. 237
- 4.13 The snapshot of 3.3 μm radial 5CB microdroplet trap at 0.2 MW/cm² at varied polarization direction, θ under cross-polarized view. The red arrows indicate the polarization direction of the trapping laser. 238
- 4.14 The schematic diagram of 5CB molecules orientation inside the microdroplet to the polarization direction of linearly polarized light. The red arrows indicate the polarization direction of the trapping laser. 238
- 4.15 The snapshot of a rotated bipolar 5CB microdroplet of 2.1 μm diameter in water by a circularly polarized laser beam. 240
- 4.16 (a) Schematic diagram of bipolar 5CB microdroplet rotates in an optical trap and (b) QPD signal of the rotated 5CB microdroplet. 240
- 4.17 The snapshot of rotated radial 5CB microdroplet of 2.9 μm diameter in water by a circularly polarized laser beam. 241
- 4.18 (a) The schematic diagram of a radial 5CB microdroplet rotates about a circle (b), which is the typical QPD signal of the rotating 5CB microdroplet. 241
- 4.19 The translation and micro-control of a single 1.8 μm bipolar 5CB microdroplet by a linearly polarized laser beam at 0.2 MW/cm². A: The 5CB microdroplet was trapped in the optical trap at $t_1 = 1$ s. B: The 5CB microdroplet translation 5 μm to the right at $t_2 = 10$ s. C: The 5CB microdroplet retrapped at $t_3 = 15$ s. D: The 5CB microdroplet translation 5 μm to the left at $t_4 = 25$ s. E: The 5CB microdroplet retrapped at $t_5 = 27$ s. 243



- 4.20 The translation and micro-control of a single $1.8 \mu\text{m}$ bipolar 5CB microdroplet by a circularly polarized laser beam at 0.2 MW/cm^2 . A: The 5CB microdroplet was trapped and rotated in the optical trap at $t_1 = 1 \text{ s}$. B: The 5CB microdroplet translation $5 \mu\text{m}$ to the right at $t_2 = 10 \text{ s}$. C: The 5CB microdroplet retrapped and rotated at $t_3 = 13 \text{ s}$. D: The 5CB microdroplet translation $5 \mu\text{m}$ to the left at $t_4 = 25 \text{ s}$. E: The 5CB microdroplet retrapped and rotated at $t_5 = 28 \text{ s}$. 243
- 4.21 (a) The x -axis trajectory of the trapped bipolar 5CB microdroplet is in Figure 4.19 and (b) in Figure 4.20. 245
- 4.22 The translation and micro-control of a single $3.3 \mu\text{m}$ radial 5CB microdroplet by a linearly polarized laser beam at 0.2 MW/cm^2 . A: The 5CB microdroplet was trapped in the optical trap at $t_1 = 1 \text{ s}$. B: The 5CB microdroplet translation $5 \mu\text{m}$ to the right at $t_2 = 10 \text{ s}$. C: The 5CB microdroplet retrapped at $t_3 = 11 \text{ s}$. D: The 5CB microdroplet translation $5 \mu\text{m}$ to the left at $t_4 = 25 \text{ s}$. E: The 5CB microdroplet retrapped at $t_5 = 28 \text{ s}$. 246
- 4.23 The translation and micro-control of a single $3.3 \mu\text{m}$ radial 5CB microdroplet by a circularly polarized laser beam at 0.2 MW/cm^2 . A: The 5CB microdroplet was trapped and rotated in the optical trap at $t_1 = 1 \text{ s}$. B: The 5CB microdroplet translation $5 \mu\text{m}$ to the right at $t_2 = 10 \text{ s}$. C: The 5CB microdroplet retrapped and rotated at $t_3 = 13 \text{ s}$. D: The 5CB microdroplet translation $5 \mu\text{m}$ to the left at $t_4 = 25 \text{ s}$. E: The 5CB microdroplet retrapped and rotated at $t_5 = 32 \text{ s}$. 246
- 4.24 (a) The x -axis trajectory of the trapped radial 5CB microdroplet is in Figure 4.22 and (b) in Figure 4.23. 248
- 4.25 Graph of corner frequency (f_c) versus optical power density (P) for (a) bipolar and (b) radial. 251
- 4.26 Graph of corner frequency per microdroplet radius ($\frac{f_c}{r}$) versus optical power density (P) for (a) bipolar and (b) radial. 252
- 4.27 Graph of corner frequency per microdroplet radius ($\frac{f_c}{r}$) against microdroplet radius at varied optical power density. 255
- 4.28 The ray optics diagram of laser focus of w_0 beam waist trapped two spheres of diameter d_1 and d_2 (Malagnino et al., 2002). 256
- 4.29 Graph of angular speed (ω) versus optical power density (P) of clockwise rotation for (a) bipolar 5CB and (b) radial 5CB microdroplets. 265

- | | | |
|------|---|-----|
| 4.30 | Graph of angular speed per microdroplet radius ($\frac{\omega}{r}$) versus optical power density (P) of clockwise rotation for (a) bipolar 5CB and (b) radial 5CB microdroplets. | 268 |
| 4.31 | Graph of angular speed (ω) versus optical power density (P) of counterclockwise rotation for (a) bipolar 5CB and (b) radial 5CB microdroplets. | 270 |
| 4.32 | Graph of angular speed per microdroplet radius ($\frac{\omega}{r}$) versus optical power density (P) of clockwise rotation for (a) bipolar 5CB and (b) radial 5CB microdroplets. | 273 |
| 4.33 | The schematic mechanism of the interaction between the 5CB microdroplet with the CTAB molecules and the effect on the internal configuration inside the microdroplet. | 279 |
| 4.34 | The transition sequence changed of the bipolar 5CB microdroplet to the radial internal configuration of 1.4 μm trapped at 0.2 MW/cm^2 linearly polarized laser beam. | 283 |
| 4.35 | Graph of displacement variance (σ^2) versus time of 1.4 μm bipolar 5CB microdroplet trapped by a linearly polarized laser beam at 0.2 MW/cm^2 . | 285 |

LIST OF SYMBOLS

SYMBOLS	MEANING	UNITS
r	Radius	m
k_B	Boltzmann constant	J/K
T	Temperature	K
F_g	Gradient force	N
F_s	Scattering force	N
D	Diameter	m
λ	Wavelength	nm
n	Refractive index	---
F_r	Restoring force	N
σ^2	Displacement variance	V ²
k	Optical stiffness	pN/ μ m
f_c	Corner frequency	Hz
ω	Angular speed	Hz
Γ	Optical torque	Nm
P	Optical power density	MW/cm ²

LIST OF CONSTANT

SYMBOLS	MEANING	UNITS
π	Pi constant	
k_B	Boltzmann constant	J/K



LIST OF ABBREVIATIONS

ASCII	American Standard Code for Information Interchange
CCD	Charged Couple Device
NA	Numerical Aperture
PSD	Power Spectrum Density
QPD	Quadrant-Photodiode
WD	Working distance
ET	Equipartition Theorem
BS	Boltzmann Statistics
NLCM	Nematic Liquid Crystal Microdroplet
PDMS	Polydimethylsiloxane
LC	Liquid Crystal
SDS	Sodium Dodecyl Sulfate
CTAB	Centrimonium Bromide





APPENDIX LIST

- A Knowledge Dissemination
- B System Specification
- C Corner Frequency per Microdroplet Radius Comparison
- D Angular Speed per Microdroplet Radius Comparison



CHAPTER 1

INTRODUCTION

1.1 Research Background

The light radiation pressure exerts a force when it comes into contacts with a particle. The force that arises from the light radiation pressure is called optical force. The optical force was applied in an instrument called optical tweezers. Arthur Ashkin, the pioneer of optical trapping, was awarded the 2018 Nobel Prize in Physics for his invention of optical tweezers for biological applications (Goswami, 2018). Optical tweezers use a strong, focused laser beam to confine the particle by benefiting optical force. Optical



forces mainly contributed to the pulling gradient force and pushing scattering force in optical trapping.

It is possible to manipulate small objects in the range of micrometers or smaller using light by optical tweezers (Malmqvist & Hertz, 1992; Pai, Zandrini, Mart, & Bragheri, 2018). The intense focus laser beam creates an optical trap where it provides non-contact micro-manipulation of a non-destructive technique of the trap particle. Subsequently, optical trapping provides minimization of the sample flaw, especially when handling soft and fragile particles like biological material. Optical trapping not only provides manipulation of the trap particle but also provides several applications. In the context of optical trapping applications, it is possible to conduct physical measurements such as viscosity, stiffness, and elasticity for example, DNA, with the help of polystyrene or silica probing (Buosciolo et al., 2004; Müllenbroich et al., 2013). The study of the microparticle trajectory by the optical trapping is useful for microrheological measurement (Aziz et al., 2015). These are the several applications performed by the optical trapping.

Optical trapping is also used in the chemistry field. This process is called laser trapping. Laser trapping application involves the system domain from quantum-scale atom trapping to the micro-scale system (David et al., 2013; Neves et al., 2015). Laser trapping shows a novel potential for light-matter interaction in molecular systems by triggering nucleation-induced crystallization growth and supramolecular assemblies (Sugiyama et al., 2012; Supian et al., 2010). Figure 1.1 (left) illustrates the laser trapping principle, while Figure 1.1 (right) illustrates the trapping assembly of



nanoparticles, polymers, and molecular clusters. The red parabolic line represents the optical potential energy in the sample.

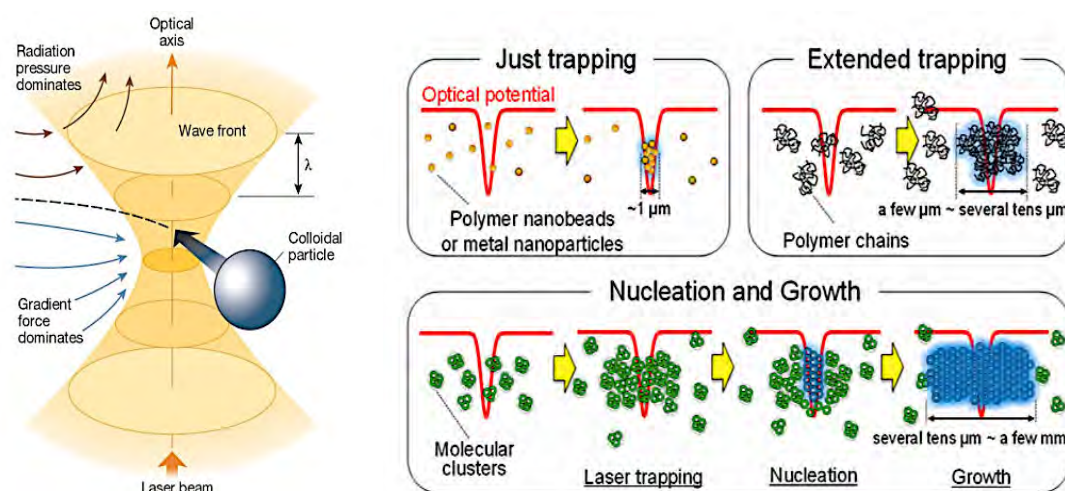


Figure 1.1. (Left) Laser trapping principle. (Right) Schematic representations for the trapping and assembly of nanoparticles, polymers, and molecular clusters. [Adapted from (Sugiyama et al., 2012).]

The application of laser trapping can be classified into Just trapping, Extended trapping, and Nucleation and Growth. The “Just trapping” refers to the laser trapping of polymers that occurs within the laser spot size in the range of $\sim 1 \mu\text{m}$. The “Extended trapping” of polymer chains can occur within a few to several tens microns beyond laser spot size due to the nature of the polymer, for example, due to intermolecular interactions. Lastly, in the context of nucleation and growth, nucleation is induced, resulting in a large crystal scale from several ten microns to a few millimeters. The extension of optical trapping beyond just trapping capability has opened a new direction in molecular control using light.

Recently, the optical trapping has shifted from trapping solid matter to soft matter, such as liquid crystals. Liquid crystal has unique properties where it co-exists in between solid and liquid states, anisotropic, birefringent, and sensitive to electric and magnetic fields (Brasselet & Juodkazis, 2009; Phanphak et al., 2014). Optical trapping of the liquid crystal can be performed in the form of a liquid film or a microdroplet (Brasselet, 2008; Brasselet et al., 2003). Interestingly, liquid crystal obtains multiple domain configurations, such as nematic, smectic, and cholesteric, which are sensitive to the light polarization state (Brasselet & Juodkazis, 2009). 4'-Pentyl-4-cyanobiphenyl (5CB) is one of the most attractive nematic liquid crystals (NLC) as it exhibits liquid crystal properties of nematic phase domain at room temperature (18–35 °C) (Hanemann et al., 1995). Therefore, 5CB is a suitable model compound to study the physical behavior of simple nematics. Figure 1.2 shows the

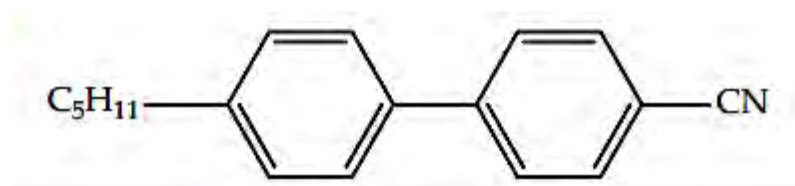


Figure 1.2. 5CB chemical structure. Adapted from (Yeng, Ayop, & Sasaki, 2022).

The dispersion of liquid crystals with an immiscible solvent such as water creates liquid crystal droplets. For example, 5CB produces a nematic liquid crystal droplet in water. In droplet form, the nematic liquid crystal has a unique internal configuration. Internal configuration refers to the domain alignment within the nematic liquid crystal droplet. The internal configuration can be controlled by surface modification with a surfactant. Tailored polarization of light can manipulate a single

nematic liquid crystal microdroplet (Usman et al., 2011). Figure 1.3 shows an example of the internal configuration of a nematic liquid crystal microdroplet.

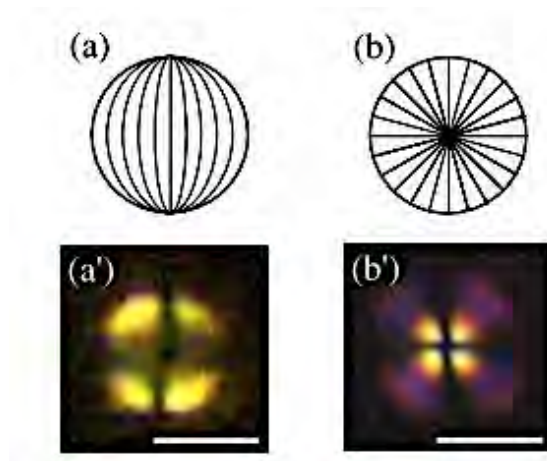


Figure 1.3. Liquid crystal internal configuration in a nematic liquid crystal microdroplet (a) bipolar and (b) radial. Observation under cross-polarization view [Adapted from ((Brasselet & Juodkazis, 2009))].

Optical trapping of nematic liquid crystal microdroplets is possible when the refractive index of the droplet is larger than the surrounding refractive index. Instead of using solid silica and polymer particles, an optically engineered liquid crystal microdroplet is flexibly shaped, allowing rotational control when exposed to the light polarization during optical trapping (Pai et al., 2018). This proposed study will help to design microfluidic devices that integrate liquid crystals as optically controlled microactuators in water filtration devices, lab-on-chips, liquid crystal-based sensors, or new technologies.

As sensitive sensors, liquid crystal droplets are indispensable in environmental and biomedical science (Niu et al., 2016). This is because liquid crystal droplets are a potential optical, biological sensor due to high birefringence and high sensitivity of



liquid alignment of liquid crystal molecules to minute variation on the surface. Molecular events occurring at an interface between liquid crystal and water can be amplified and converted into electrical signals by the change in orientation of liquid crystal molecules, which are visible to the naked eye under a polarizing microscope (Niu et al., 2016). The liquid crystal-based sensor can detect proteins, nucleic acids, acetylcholine, glucose, enzymes, cholic acid, antibodies, and other molecules during sensing application.

1.2 Problem Statement

Optical tweezers are commonly used to trap and manipulate particles in a liquid. For example, most microscopic biological particles must be trapped within the liquid.

Recent studies showed that microparticles in liquids can form two-dimensional structures by laser guidance (Kudo et al., 2016; Shih et al., 2021; Wu et al., 2018). However, it was experimentally successful with gold nanoparticles and polystyrene beads, even if the theoretical explanation of the observed phenomena is not yet mature. One hypothesis states that the lattice-like arrangement is due to light propagation through the dielectric properties of the trapped particles. Liquid crystals can have both solid-like and liquid-like properties. The magnetic, electrical, and optical methods can control the internal configuration inside the liquid crystal droplet. The physical properties of liquid crystals depend highly on the alignment of liquid crystal molecules in a closed cell. The study of optical trapping utilizing light propagation catalyzes new pathways in the assembly, manipulation, and crystallization



of microparticles, nanoparticles, supramolecules, and soft matter, as anticipated in this study.

The previous researcher reports that the general formulation of nematic liquid crystal microdroplet production thus leads to a reproducibility problem (Choi et al., 2015; Juodkazis et al., 1999; Lee et al., 2015; Murazawa, S. Juodkazis, 2005; Suga et al., 2018; Z. Wang et al., 2020). There are no specific formulations, recipes, or technical reports to prepare nematic liquid crystal microdroplets. The reported nematic liquid crystal microdroplet was relatively large ($>10\text{ }\mu\text{m}$) (Duan et al., 2019; Kiang-Ia et al., 2021; Shechter et al., 2020). The nematic liquid crystal microdroplet must be a small, miniaturized version of the liquid crystal-based probe. The bigger liquid crystal microdroplet is inert with a small optical force in optical trapping application. The smaller probe can increase surface volume sensitivity for sensing applications.

Furthermore, although previous researchers reported optical trapping of a single nematic liquid crystal microdroplet, they only reported qualitative observation of nematic liquid crystal microdroplet trapping by studying the behavior of the trapped liquid crystal microdroplet under light polarization (Phanphak et al., 2014; Shechter et al., 2020; Usman et al., 2013). No study quantifies the change in the internal configuration of the nematic liquid crystal microdroplets in terms of optical signal but instead just observing the changes visually (Murazawa, Juodkazis, Matsuo, et al., 2005; Shechter et al., 2020). The study of the optical stiffness of nematic liquid crystal microdroplets based on the optical which is relevant for evaluating the strength of the optical trap, is also not reported. Hence, there is a lack of information on the trend of



optical stiffness with exposure to different optical power densities and microdroplet sizes for soft matter optical trapping.

In addition, the optical manipulation of the liquid crystal microdroplet has been reported on the dynamic behavior when the laser polarization state used is varied (Saito & Kimura, 2022). However, there is no combination of simultaneous translational and polarization control of liquid crystal microdroplet has been reported. This combination is expected to enrich liquid crystal microdroplets for actuating application. In the context of rotational study, the laser power used is larger, and the size of the microdroplet is bigger, as reported by previous researchers. This becomes an issue when the use of strong laser power tends to destroy the liquid crystal nematic phase, and bigger microdroplets are challenging to actuate in tiny areas of actuation. Hence, there is a requirement to reduce laser power and microdroplet size for actuating application using liquid crystal microdroplet trapping.

The conventional liquid crystal-based sensor observes the transition liquid crystal configuration without converting the changes into a quantitative signal, possibly causing the false judgment when the liquid crystal microdroplet is smaller (Lee et al., 2015; Niu et al., 2016). The existing liquid crystal-based sensor requires many large liquid crystal droplet sizes for detection because the detection is based on the internal configurational change of bigger microdroplets (Lee et al., 2015; Niu et al., 2016). The current liquid crystal-based sensor applied a lasing technique to increase the detection sensitivity by using only a single microdroplet. However, the microdroplet used for detection is stuck on the glass slide or hung at the end of the micro syringe which causes deformation in shape because of poor control, immobilize and bigger droplet size,



leading to a reduction in sensitivity (Duan et al., 2019; Duan, Hao, et al., 2020; Duan, Li, et al., 2020). Determining the properties of liquid crystal-based probes is essential for future use in microactuators and microsensors in liquids.

This study uses a nematic liquid crystal microdroplet solution. The challenge of this study is to produce a nematic solution with a homogeneous size with a specific internal configuration in the 5CB microdroplet and quantifying the optical manipulation of 5CB microdroplet due to the nature of soft matter. The molecular alignment that determines the internal configuration is possible by inducing surface modification of the microdroplets. Furthermore, this study develops the optical manipulation of a single microdroplet for a liquid-crystal-based actuator and a liquid-crystal-based sensor involving optical signal transition in a liquid-crystal configuration

 05-4506832
  pustaka.upsi.edu.my
  Perpustakaan Tuanku Bainun
Kampus Sultan Abdul Jalil Shah
  PustakaTBainun
  ptbupsi

1.3 Research Objective

This study aims to optically trap and manipulate 4-Cyano-4'-pentylbiphenyl (5CB) microdroplets in water. The objectives of the study are:

1. To formulate the production of 5CB microdroplets within a suitable range to be optically trapped.
2. To optically trap a single 5CB microdroplet in water within a suitable size range using 976 nm laser.
3. To optically micro-control a single 5CB microdroplet in water using a circularly polarized laser.



4. To quantitatively determine factors that affect the optical manipulation of the 5CB microdroplet for actuating and sensing applications.

1.4 Significance of Research

This research examines the optical trapping array of nematic liquid crystal microdroplets. This research studies and observes the interaction of light with 5CB microdroplets. It explains the physical interaction between 5CB micro-droplets for non-contact micro-actuators in liquid crystal-based sensor applications.

In addition, the importance of this research lies in the polarization control of light using 5CB microdroplets. This study hypothesizes that light polarization affects the capture of 5CB microdroplets as they are prone to a light polarization state. Varying the laser polarization state used leads directly to a change in the intrinsic configuration of the 5CB microdroplet. The cross-polarization view and electrical signal from QPD observe and detect intrinsic configurational changes within the 5CB microdroplet.

Because liquid crystal is inherently birefringent, this study assumes that the optical strength of 5CB microdroplet capture varies with the polarization state of the capture laser at the same optical density. In addition, due to internal light loss and light loss at the interface, it is expected that the optical strength is not constant for all 5CB microdroplet sizes in the tuned range.



The optical signal change of the internal configuration of the 5CB microdroplet is characterized in the context of corner frequency and optical stiffness measurements. This finding is crucial for application in microactuators and sensor applications. Determining optical stiffness is useful for precisely controlling liquid crystal-based probe applications because optical stiffness shows the trend of the optical trapping with respect to varied parameters such as laser power and microdroplet size. Hence, the researcher can predict the suitable laser power and probe size for prospective application. In addition, optical stiffness measurement results are expected to vary for the internal configuration of bipolar and radial 5CB microdroplets. This finding helps to precisely characterize the transient change of liquid crystal-based sensors especially during the transitional change from bipolar to the radial internal configuration of liquid crystal microdroplets, to determine the significant difference to be applied for quantitative sensing mechanism, instead of observing them visually, in the microsensor application.

1.5 Limitation of Research

This study focuses on 5CB microdroplet trapping. The phase selected for trapping is nematic. The single droplet in the nematic phase is optically captured. 5CB is used as the primary liquid crystal to produce a 5CB microdroplet. As already mentioned, 5CB exists as a liquid crystal at room temperature; Thus, it instantly creates 5CB microdroplets in the water. Deionized water is chosen as the primary liquid for optical capture. Other liquid crystals could exist as a pure solids or liquids at room



temperature, which is unsuitable for producing microdroplets. Therefore, the 5CB is dispersed and homogenized in deionized water at room temperature.

The laser tweezers optically trap a single 5CB microdroplet in water with a radius of 0.6 μm to 3.7 μm . The 5CB micro-droplet radius of less than 0.5 μm is challenging to see clearly under the CCD camera due to the resolution limitation of the optical tweezers. In addition, capturing more than one droplet at a time can be problematic as it disrupts the 5CB optical signal. Subsequently, the internal configuration of the 5CB microdroplets is focused on the bipolar and radial configurations.

The optical trapping process of this experiment depends on the optical tweezers OTKB(/M). Furthermore, the setup of the optical trap of this experiment depends on the oil immersion objective lens (NA 1.25, 100 \times) and the optical resolution \approx of 500 nm. Optical resolution is the limitation of the instrument used to perform optical capture. The laser power ranges from 0.2 MW/cm² to 7.3 MW/cm². The lower laser power is essential for capturing 5CB microdroplets sensitive to temperature changes. Too much laser power severely destroys the nematic phase of the 5CB microdroplet.



1.6 Thesis Outline

This thesis essentially consists of 5 chapters. Chapter 1 provides the background to the study and the direction and goal of the research. The central part of this chapter is the problem and the research goal.

Chapter 2 deals with the principle of optical trapping. The theory for calibrating the optical stiffness of the optical tweezers is presented. The previous reports on the optical trapping of solid particles and liquid microdroplets are presented. The introduction of liquid crystals, and the optical capture of liquid crystals are also discussed. In addition, the use of liquid crystal microdroplets in actuator and sensor applications is also described.

Chapter 3 describes the methodology of the research. The first part of the methodology is the setup and alignment of optical tweezers. The second part involves the preparation of the 5CB microdroplet suspensions in water. The fourth part is the optical trapping of the 5CB microdroplet in water using a linearly and circularly polarized laser beam. The methodology's last part analyzes the distribution size and stability of the 5CB microdroplet suspension, the simultaneous translation and micro control, the corner frequency, the angular velocity, and the displacement variance of the captured single 5CB microdroplet.

In Chapter 4, the results of the conducted experiment are discussed. The 5CB treatment generates the ultrasonic microdroplet and is observed under the optical microscope. The distribution size and the stability of the 5CB microdroplet are



presented. In addition, the effect of the linearly and circularly polarized laser beam on the trapped 5CB microdroplet is observed. The corner frequency and angular velocity of the trapped 5CB microdroplet are discussed. In addition, the transitional change in the internal configuration of 5CB is quantitatively calculated and presented.

Chapter 5 discusses the conclusion of the research findings on the research findings. Finally, recommendations are given to improve and expand the research for further studies.

1.7 Summary

This chapter presents the background of the study, the problem, the research goals, the importance of the research, and its limitations.